JES Focus Issue on Semiconductor Electrochemistry and Photoelectrochemistry in Honor of Krishnan Rajeshwar

The Impact of Different Si Surface Terminations in the (100) p-Si | n^+-Si | Cu Junction with Respect to the Photo Electrochemical Performance

Céline Steinert,[z] Sven Tengeler, Bernhard Kaiser, and Wolfram Jaegermann

Institute for Materials Science, Technical University of Darmstadt, 64287 Darmstadt, Germany

The (100) p-Si | n^+-Si | Cu interface is investigated with respect to the electronic band structure and the electrochemical performance. Thin layers of metallic copper were deposited stepwise by E-beam deposition and analyzed in-line by XPS after each deposition step. For this purpose, different silicon surface terminations were prepared: hydrogen termination, thermal oxide (7 Å) and native oxide (3 Å). After contact formation the initial flatband situation of the n^+-Si layer changes to an upward band bending depending on the Si surface termination: 0.45 eV for the H termination, 0.35 eV for the native oxide and 0.27 eV for the thermal oxide. The electrochemical performance measured by cyclic voltammetry for each junction correlates to the respective energy band alignment. While the H terminated surface with the highest upward band bending leads to the worst electrochemical performance, the surface passivated with thermal oxide and the lowest upward band bending results in the best electrochemical performance. For the two passivated surfaces, the thickness of the passivating oxide layer may also be an issue. The Si surface with a thicker thermal oxide (7 Å) shows better band alignment and electrochemical performance compared to the Si surface with a thinner native oxide (3 Å).
 [DOI: 10.1149/2.0291905jes]

Manuscript submitted October 18, 2018; revised manuscript received January 23, 2019. Published February 5, 2019. *This paper is part of the JES Focus Issue on Semiconductor Electrochemistry and Photoelectrochemistry in Honor of Krishnan Rajeshwar.*

Due to worldwide growing industrialization, the energy demand has been drastically increased within the last decades. In order to preserve our environment and limit global warming, the development of efficient renewable energy sources is urgently needed. However, wind and solar power as most promising alternative sources suffer from their inherent volatility with strongly variable energy fluxes with time, which are not in phase with the societal consumption needs. Storable and transportable fuels from renewable energies are essential. Here, natural photosynthesis, which is the most important and prototype method of harvesting solar energy,[1] acts as natural role model. Photoelectrochemical cells may develop to a key technology, especially when they will be able to convert CO_2 directly into fuels, using sunlight. The first essential part of such a device is the photoabsorber, which has to drive the photoelectrochemical reaction. In the model system presented here, a (100) p-Si | n^+-Si junction serves as photoabsorber material which will be compared to bare p-Si. Another important part of the photoelectrochemical device is an appropriate catalyst which allows high current densities at low overpotentials when being in contact to an electrolyte. As Cu is known to be able to reduce CO_2 to CO, CH_4, C_2H_4 and alcohols in aqueous electrolytes,[2–6] Cu is used as prototype catalyst for the present study as well. For CO_2 reduction the use of Si based multijunction solar cells directly inserted into the electrolyte is planned. However, because of limited multijunction sample availability the PV/electrolyser coupling was investigated first using single crystalline Si as model substrate.

Especially in the last years there have been a lot of publications in the field of CO_2 reduction. While Urbain[7] et al. used Cu foam connected by wires to a Si solar cell for the electrochemical CO_2 reduction reaction (CRR), a CuAg cathode was used by Gurudaya[8] et al. Furthermore, solar energy conversion was realized by Sugano[9] et al. with a wired photovoltaic photoelectrochemical system with Au nanoparticles as the CRR active cathode. Also, Au thin films have been proven to work as catalyst to form CO as CRR product.[10] Besides Cu and Au, further catalyst materials have been utilized for the CRR e.g. IrOx,[11] Ru,[12] Cr, Mo and W.[13] However, the deposition of a catalytic active thin film directly onto the semiconductor surface has not been investigated in a systematic way so far. In a first step Cu as most promising CRR catalyst is used for this purpose. $KHCO_3$ is employed as appropriate electrolyte in all performed experiments as described in previous work.[14–18] One major condition for an effective system is the successful coupling of the PV component to the electrolysis component without any losses in photo current (recombination) and photo voltage (energy alignment) across the interface.

The present study demonstrates that the electrochemical performance of an integrated photoelectrochemical device can be predicted and optimized by investigating the electronic structure at the interface between its two main parts: the Si junction as the photoabsorber and the Cu as the catalytically active layer. For this reason this interface was investigated by in-line X-ray photoelectron spectroscopy (XPS) analysis after the stepwise deposition of Cu on the Si surfaces with different surface terminations. At first, bare p-doped Si wafers were used as reference before analyzing the (100) pn^+-Si junctions. Furthermore, cyclic voltammetry was used to determine the electrochemical performance of each system. With this approach a basic understanding on how the different band alignments due to different surface terminations impact the CRR is achieved. Similar characterization experiments were also reported for the oxygen evolution reaction recently.[19]

Experimental

Sample preparation.—The experiments were performed on 1 cm × 1 cm pieces of 100 mm diameter (100) boron doped p-type silicon wafers ($p = 10^{16}$ cm^{-3}) with and without a 50 nm thick arsenic doped n^+-type silicon layer on top ($n = 10^{19}$ cm^{-3}). All samples were first cleaned in an ultrasonic bath for 10 min in acetone, isopropanol and MilliQ water. For the Si surface termination with native oxide no further preparation steps were necessary. For the hydrogen terminated Si surface the sample was first etched in piranha solution (H_2SO_4:H_2O = 2:1) at 80°C for 10 min and afterwards in 5% HF also for 10 min. After another etching step in freshly prepared piranha for again 10 min at 80°C, the sample was finally etched for 10 min in 40% NH_4F at room temperature.[20] In between each step the sample was thoroughly rinsed with MilliQ water. Afterwards, the sample was introduced into ultra high vacuum (UHV) at the Darmstadt Integrated System for Fundamental research (DAISY Fun).[21] In order to obtain thermally grown oxide a sample with a H terminated surface was introduced to a deposition chamber of the DAISY Fun where it was held in a mixed oxygen argon atmosphere (50 sccm O_2, 50 sccm Ar, 0.1 mbar) for 45 min at 800°C.

[z]E-mail: csteinert@surface.tu-darmstadt.de

Interface experiments.—Before depositing the first layer of Cu on the differently prepared Si samples, the bare substrates were analyzed by XPS in order to check if the surface is free of any contaminations. Afterwards the samples were transferred into a deposition chamber where a thin layer of Cu was deposited by electron beam deposition at pressures of 10^{-7} mbar or better. Subsequently, the samples were analyzed again by XPS followed by another Cu deposition and so on, until the Cu 2p emissions became dominant and the Si substrate was barely visible any more. The XPS measurements were all performed at a pressure of 5×10^{-10} mbar or better using a Specs Phoibos 150 setup (Focus 500 with XR50M). For all measurements a monochromatic Al K_α line of 1486.64 eV was used as X-ray excitation. Survey measurements were obtained with a pass energy of 20 eV while all detail spectra were measured with a pass energy of 10 eV. The spectrometer was calibrated against the Cu 2p, Ag 3d and Au 4f core levels as well as the valence band edges. As evaluation software Igor Pro was used.

To calculate the band bending before and after contact formation the Si $2p_{3/2}$ emission line needs to be analyzed. For the initial band alignment the position of the corresponding Si $2p_{3/2}$ emission line is determined. Accordingly, the distance between the valence band to the Fermi level can be determined by subtracting the known value of E_B(VB)-E_B(Si $2p_{3/2}$) of 98.74 eV from the measured value of the Si $2p_{3/2}$ emission line (E_B'(Si $2p_{3/2}$)). Additionally, the distance between conduction band and Fermi level is defined by the effective density of states as well as the doping concentration. This correlation is given by

$$E_{CB} - E_F = kT\ In\left(\frac{N_{CB}}{n}\right)$$

where N_{CB} is the effective density of states (DOS) in the conduction band and n the doping concentration. Finally, both derived values are subtracted from the known value of the Si bandgap ($E_g = 1.12$ eV) which results in the band bending E_b

$$E_b = 1.12\ eV - \left(98.74\ eV - E_B'\left(Si\ 2p_{3/2}\right)\right) - \left(E_{CB} - E_F\right).$$

Analogous to this approach the band alignment after contact formation can be determined when evaluating the measured XP spectra after the last Cu deposition step.

Determination of film thickness.—The film thickness was determined by the numerical solution of

$$\frac{I_{Cu}}{I_{Si}} = \frac{N_{Cu}}{N_{Si}} \frac{1 - \exp\left(\frac{-d_{Cu}}{\lambda_{Cu}(E_{kin,Si})cos\partial}\right)}{\exp\left(\frac{-d_{Cu}}{\lambda_{Cu}(E_{kin,Si})cos\partial}\right)}$$

for the thin Cu layer on the bulk Si substrate.[22,23] Here, I_{Cu} and I_{Si} are the integrated core level line intensities which are corrected with a Shirley background.[24] λ_{Cu} and λ_{Si} are the inelastic mean free paths (IMFP) for the kinetic energy of the electrons in the thin surface layer. Cu and N_{Cu} as well as N_{Si} are the materials atomic densities. The electron emission angle is defined as ∂. In order to determine the layer thickness of the oxide, the initial Si 2p peak intensity needs to be taken into account. In order to remove the background of the spectrum a Shirley background correction has been applied. Additionally to the Si 2p peak the SiO_2 peak can be seen at 103.5 eV (literature: 103.2 eV).[25] For calculating the layer thickness d of the SiO_2 the relation of the integrated core level lines I_{Si2p} and I_{SiO2} needs to be taken into account. Furthermore, the materials atomic densities N_{Si} and N_{SiO2}, the inelastic mean free path λ of SiO_2 and the electron emission angle ∂ are defining the layer thickness as shown in the following equation

$$d_{SiO_2} = \lambda_{SiO_2} \cos\partial \ln\left(1 + \frac{I_{SiO_2} N_{Si}}{I_{Si} N_{SiO_2}}\right).$$

For the native oxide a layer thickness of 3 Å and for the thermal oxide a thickness of 7 Å was calculated.

Electrochemical experiments.—After completing the interface experiments the samples were extracted from UHV in order to perform photo electrochemical (PEC) measurements. For electrical back contacts GaIn (Alfa Aesar, 99.99% pure) was scratched into the substrates[26–28] and then the sample was inserted into an EC cell from Zahner (PECC-2). As electrolyte 0.3 M $KHCO_3$ was filled into the EC cell after calibrating an Ag/AgCl reference electrode against a reversible hydrogen electrode (RHE). The calibrated reference electrode was used in a standard three electrode setup controlled by the potentiostat (Zennium, PP221 Zahner-Elektrik). The cyclic voltammetry (CV) measurements were performed under illumination or with chopped light with illuminated time intervals of four seconds. As light source a LED with a wavelength of 625 nm was used which was operated with a power of 180 W/m^2.

Results and Discussion

Previous to the extensive characterization of different pn$^+$-Si | Cu interfaces a p-Si | thermal oxide | Cu sample was investigated as reference system. The aim of using this very basic model sample was to obtain a systematic understanding of the electronic and catalytic properties of Si | Cu interfaces. However, we expect that advanced model systems containing buried junctions such as pn$^+$-Si | Cu and pin-Si | Cu will be desired as integrated photo electrochemical device and therefore we have put our emphasis on such systems.

p-Si | Cu interfaces.—As a first reference system the electronic band structure of p-Si | thermal oxide | Cu was investigated by a XPS interface experiment. The corresponding XP spectra are attached in the supplementary information figure S 1. This step is important in order to understand the basic model system before coming to the more complex system of pn$^+$-Si junctions in contact with Cu as catalyst. The determined band alignments of p-Si | thermal oxide before and after contact formation with Cu are shown in Figure 1. Here, Figure 1 A shows the initial situation before contact formation. For the thermal oxide there is a large downward band bending of 0.4 eV which is also found after extensive preparation steps as etching to form H terminated surfaces or subsequent oxidation to form a thermal oxide. A preferable flatband situation is not achieved in our experiments, which is due to midgap defects at the p-Si surface and Fermi level pinning as a consequence. In Figure 1B it can be seen that for the p-Si | thermal oxide sample the band bending is slightly reduced from 0.4 eV to 0.3 eV when brought into contact with Cu. Presumably the band alignment after contact formation is not determined by the Cu contact but by the initial Fermi level pinning. In such cases, which are expected to be the dominating case for most experiments using Si as substrate, the contact properties to a metal as e.g. a Cu thin film deposited onto a p-Si | thermal oxide sample will be dominated by Fermi level pinning.[29–32]

The photo electrochemical performance of the p-Si | thermal oxide | Cu reference sample is shown in Figure 2. The displayed chopped light CV shows the difference between the CV measurements under illumination and in the dark. First, it can be pointed out that the sample does not show a classic chopped light behavior as the dark current density reaches values below-1 mA/cm^2 for potentials smaller than −0.9 V vs. RHE. This behavior differs from expectations for an ideal Schottky barrier.[19,33] The reason for this behavior is the occurrence of Fermi level pinning at midgap position which is already evident from the p-Si | SiO_2 surface before contacted to Cu (Fig. 1). The remaining midgap defects in the Si | SiO_2 phase boundary lead to effective tunneling across the junction without sharing the desired diode behavior across the interface. The p-Si | thermal oxide | Cu junction represents a basic model system, which is not expected to supply enough current to drive the CRR.

pn$^+$-Si | Cu interfaces.—In order to analyze the initial electronic band structure of the three different Si surface terminations prior to Cu deposition and to verify whether the surfaces are free of contaminations, survey spectra were measured by XPS, as displayed in

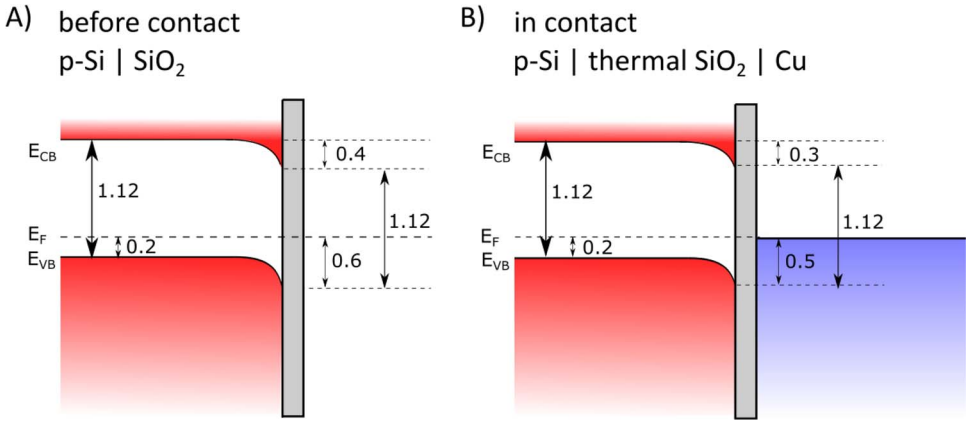

Figure 1. Energy band diagrams of bare p-Si before and after contact formation. A) p-Si | SiO_2 before contact formation with pinned Fermi level and initial band bending of 0.4 eV, B) p-Si | thermal SiO_2 | Cu with a slightly reduced band bending of 0.3 eV.

the supplemental information S 2. For the hydrogen terminated surface, the two dominant emissions are Si 2s and Si 2p with binding energies of 151.05 eV and 99.98 eV, respectively, which are in agreement to literature.[25,34–36] There is also a very small amount of oxygen present in the sample with the H terminated surface as can be deduced from the O 1s line and the O KLL Auger line at 531 eV and 979.15 eV, respectively.[37,38] The corresponding XP detail spectrum of the Cu LMM Auger line for all samples can be seen in the supplemental information S 6. The specific photoelectron lines of Si also dominate the spectra of the two samples with additional oxide layers. While the intensities of the Si 2s and Si 2p lines are comparable, the O 1s and O KLL lines are more intense for the sample with the thicker (7 Å) thermal oxide as compared the thinner (3 Å) native oxide layer. It can be concluded from figure S 2 that the H terminated sample and the sample with the thermal oxide are free of any severe contamination. The native oxide sample shows a photoelectron line at 285 eV which is specific for C 1s. As this sample did not undergo a piranha etching procedure the carbon contamination from storage in ambient air was not removed.

After this initial analysis, on all three Si surfaces with different termination, Cu was deposited stepwise, followed again by XPS analysis after each step. In Figure 3, the evolution of the XP spectra during the interface experiment is shown for the Si sample with the native oxide layer. The H terminated and thermal oxide samples are shown in Figures 4 and 5, respectively. In the corresponding survey spectra which are supplementary shown in figure S 3 only the substrate and Cu overlayer photoelectron lines appear. As there are no additional photoelectron lines visible, especially from carbon, these samples are free of any contamination. Moreover, it can be seen that the intensities of the initial oxygen and silicon lines decrease with each deposition step, and the characteristic lines for copper Cu 2s, Cu 2p and Cu LMM emerge. It can also be concluded from the Si $2p_{3/2}$, O 1s and Cu 2p emission lines that no chemical reaction occurs at the H terminated interface but at the interfaces with native and thermal SiO_2. When the detail spectra Si 2p, O1s and Cu 2p of the differently prepared pn^+-Si surfaces (see Figure 3, Figures 4 and Figure 5) are compared to each other, they basically show the same behavior and spectral features. As main difference the contribution of the SiO_2 related emission feature at around 103.5 eV is evident, its thickness will be evaluated below. Furthermore, there is a difference in the development of the O1s emission line for the H terminated surface and the surfaces with SiO_2 interlayers. While there is no oxygen reaction for the pn^+-Si:H | Cu interface, it can be observed for the interfaces with additional SiO_2 layers. Otherwise, there are some minor differences in the binding energy values due to a slightly different band energy diagram which will be also discussed in more detail below. The maximum of the Si 2p line shifts to lower binding energies due to contact formation to copper. Furthermore, it can be noticed that the initial Si 2p emission shows a minimum at 100.2 eV. This high resolution feature indicates the initial electronic flatband situation. As soon as the Si substrate is covered with Cu this minimum vanishes and additionally the entire Si 2p peak broadens. At a binding energy of 103.5 eV the SiO_2 emission is found, which also decreases with increasing Cu layer thickness. The intensity ratio of SiO_2 and Si will be discussed later. While the Si 2p peak vanishes, the Cu 2p peak increases with ongoing deposition steps.

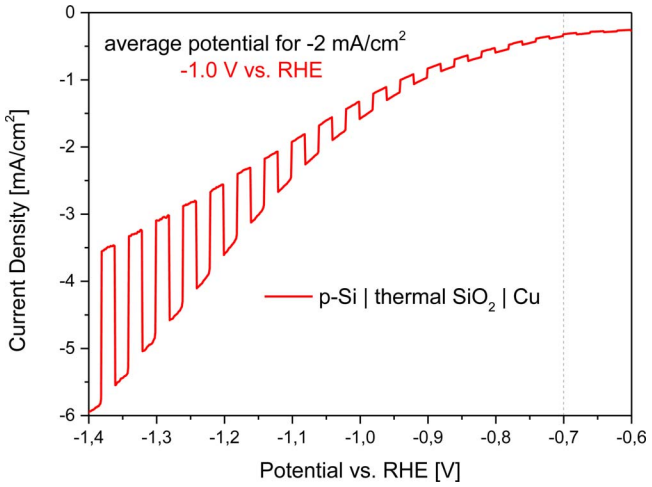

Figure 2. Cyclic voltammetry behavior of the reference system: p-Si | thermal SiO_2 | Cu under chopped illumination (4 sec interval) of 180 W/m^2 with λ = 625 nm in 0.3 M $KHCO_3$.

Within the large Cu 2p splitting the observed signal remains quite flat, which indicates the deposition of mostly metallic Cu.[39–42] Very weak satellites denote the negligible formation of Cu_2O and of CuO.[43] The Cu was deposited until a layer thickness of 81 Å was reached.

The aim of all performed XPS measurements was the investigation of the interfaces and thus of the energy band alignments of the differently treated pn^+-Si surfaces. The investigated band diagrams for pn^+-Si with and without oxide layer before and after being in contact with Cu are displayed in Figure 6. Here, fraction Figure 6 A shows the initial energetic situation of the pn^+-Si | SiO_2 before the Cu deposition. The bandgap of 1.12 eV for Si[29] is sketched as well as the distance of the Fermi level to the valence band, which is 0.2 eV. This value was determined by the solution of

$$E_F - E_{VB} = kT\ ln\left(\frac{N_{VB}}{p}\right),$$

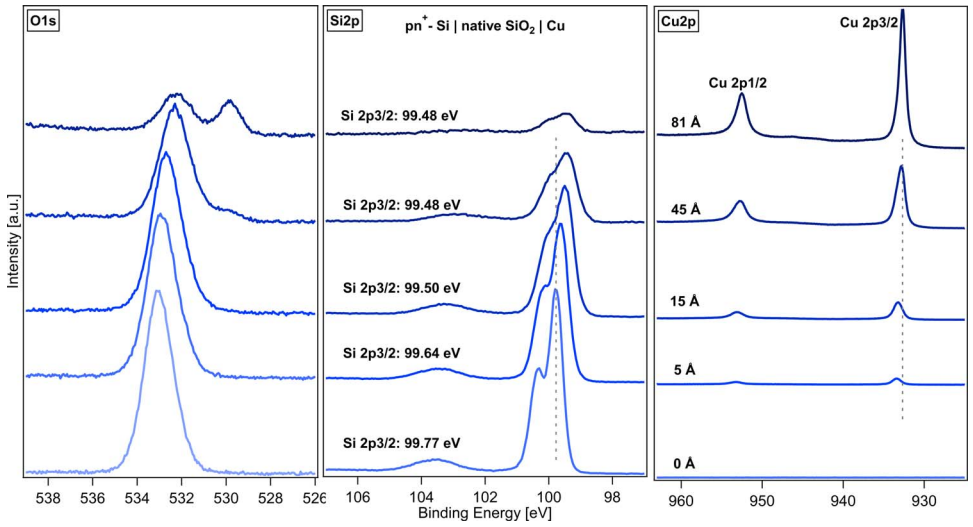

Figure 3. XP spectra of a pn^+-Si sample with a native oxide layer on top after a step wise Cu deposition. Left: changing O1s emission. Middle: decreasing Si2p emission and shift to lower binding energy with ongoing Cu deposition. Right: Emerging Cu 2p emission with increasing film thickness.

where N_{VB} is the effective density of states (DOS) in the valence band and p is the doping concentration ($p = 10^{-16}$ cm^{-3}). In the n^+-Si layer the doping concentration n is much higher ($n = 10^{19}$ cm^{-3}), which results in a very small distance of the Fermi level to the conduction band of 0.03 eV. With a slight upward band bending of 0.06 eV a flatband like situation for the n^+-Si top layer and a space charge layer between the pn^+-Si layers can be assumed as initial electronic structure. For this starting situation a Si $2p_{3/2}$ core level binding energy at 99.77 eV has been measured for the natural oxide terminated pn^+-Si surface. With the known value of E_B(VB)-E_B(Si $2p_{3/2}$) of 98.74 eV this corresponds to a value of E_F-E_{VB} of 1.03 eV in agreement to the presented energy diagram. Figure 6B shows the electronic band structure of pn^+-Si | native SiO_2 | Cu. A band bending upwards of 0.35 eV induced in the n^+ surface layer can be noticed. In case of the thermal oxide this surface band bending is smaller having a value of 0.27 eV, as can be seen in Figure 6C. The reason for the more ideal band alignment in case of the thermal oxide might be the better surface passivation due to the higher layer thickness of 7 Å compared to only 3 Å for the native oxide. Furthermore, different properties of the oxide layers may play an additional role. For the hydrogen terminated system the initial electronic structure before the Cu deposition is illustrated in Figure 6D. With an initial band bending of only 0.01 eV at the surface a flatband situation in the n^+ layer is given. When being in contact with Cu an upward band bending of 0.45 eV develops as illustrated in Figure 6E. These band bending changes in the topmost Si n^+ layer can directly be deduced from the different shift of the Si $2p_{3/2}$ binding energy values with Cu deposition ($E_{B\ (pn+\text{-Si | native SiO2 | Cu})}$ = 99.48 eV, $E_{B\ (pn+\text{-Si | thermal SiO2 | Cu})}$ = 99.56 eV and $E_{B\ (pn+\text{-Si:H | Cu})}$ = 99.38 eV). As the photo electrons, which come from the conduction band of the pn^+-Si junction, need to overcome the energetic barrier between n^+-Si and Cu, it is advantageous to have only a small upward band bending at this point. Thus, it can be concluded that the model system pn^+-Si | thermal SiO_2 | Cu with a barrier of only 0.27 eV provides the best electronic transport properties followed by the model system pn^+-Si | native SiO_2 | Cu with 0.35 eV and pn^+-Si:H | Cu with 0.45 eV barriers respectively.

These differences in the band energy diagrams as deduced from the XPS interface experiments were compared to additional CV

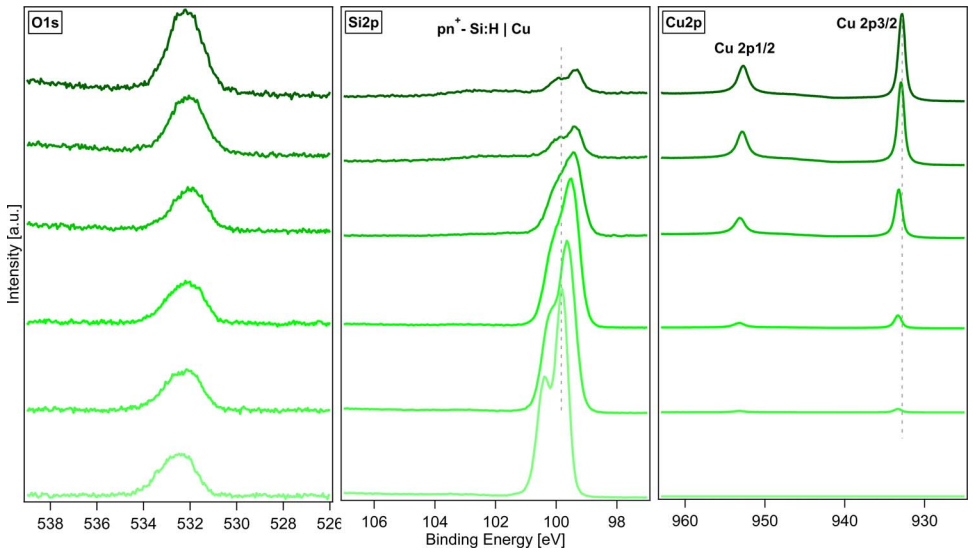

Figure 4. XP spectra of a pn^+-Si sample with a hydrogen terminated layer on top after a step wise Cu deposition. Left: changing O1s emission. Middle: decreasing Si2p emission and shift to lower binding energy with ongoing Cu deposition. Right: Emerging Cu 2p emission with increasing film thickness.

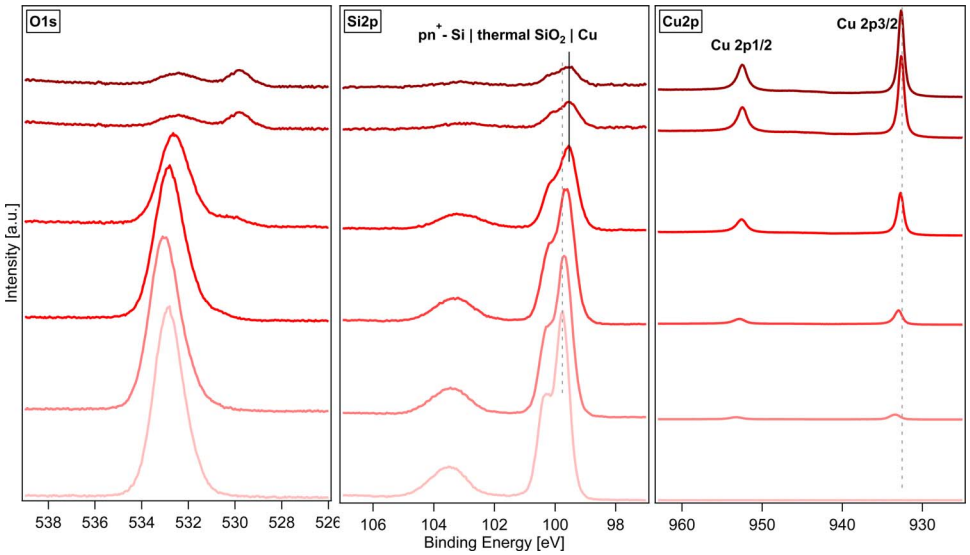

Figure 5. XP spectra of a pn^+-Si sample with a thermal oxide layer on top after a step wise Cu deposition. Left: changing O1s emission. Middle: decreasing Si2p emission and shift to lower binding energy with ongoing Cu deposition. Right: Emerging Cu 2p emission with increasing film thickness.

measurements, to determine the influence of the energy level alignment on the electrochemical performance. It is assumed that the samples with lower energetic barriers at the n^+-Si | Cu interface deliver a better performance compared to the samples with higher barriers. The catalytic performance in CV for all three systems can be seen in Figure 7. First, it can be concluded that under illumination all samples reached a similar saturation current density of -5.5 to -6 mA/cm^2 under an illumination of 180 W/m^2. But, for obtaining a current density of -2 mA/cm^2 a potential of averaged -0.7 V (vs. RHE) was necessary for the pn^+-Si:H | Cu sample. For the pn^+-Si | native SiO_2 | Cu sample a potential of -0.6 V was sufficient while the pn^+-Si | thermal SiO_2 | Cu sample was able to reach a current density of -2 mA/cm^2 at an applied potential of only -0.4 V. These results are in excellent agreement with the expectations from the investigated electronic band structure of the samples since the electrochemical performance is improved for low band bendings after contact formation. Additionally, the layer thickness of the intermediate SiO_2 can be discussed. While the native oxide has only a thickness of 3 Å, the thermally grown oxide layer is 7 Å thick. As a thicker thermal oxide layer results in a better surface passivation compared to a thinner

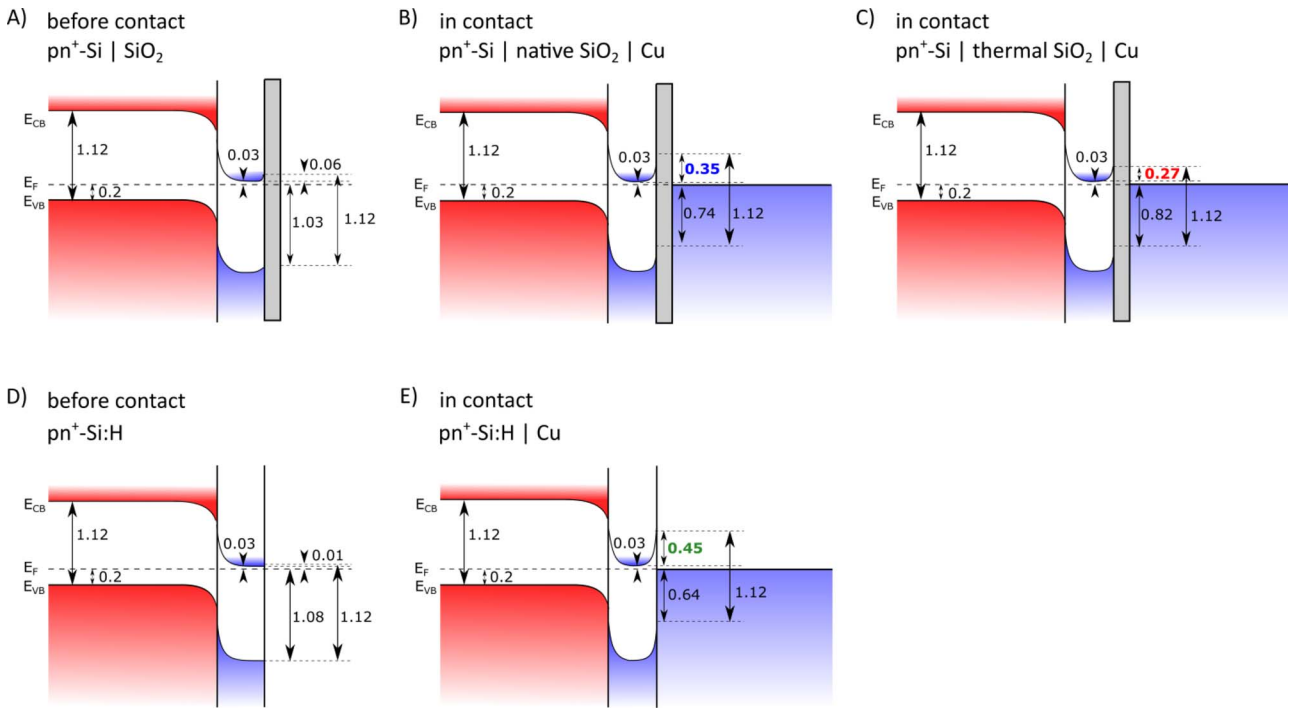

Figure 6. Energy band diagrams before and after contact formation. A) pn^+-Si | SiO_2 before contact formation with flatband like situation, B) pn^+-Si | native SiO_2 | Cu with an upward band bending of 0.35 eV, C) pn^+-Si | thermal SiO_2 | Cu with an upward band bending of 0.27 eV, D) pn^+-Si:H before contact formation with flatband situation and E) pn^+-Si:H | Cu with an upward band bending of 0.45 eV. Due to the differences in the band alignments, different electrochemical performances are expected.

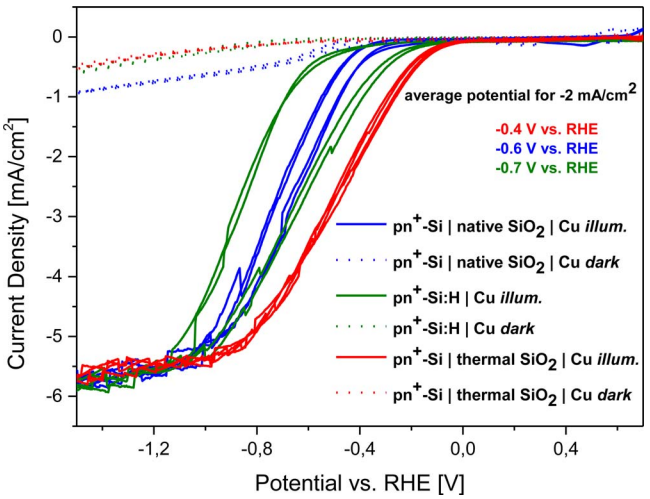

Figure 7. Comparison of the cyclic voltammetry behavior of the three different model systems: pn^+-Si | native SiO_2 | Cu, pn^+-Si | thermal SiO_2 | Cu and pn^+-Si:H | Cu under an illumination of 180 W/m^2 with $\lambda = 625$ nm in 0.3 M $KHCO_3$. Solid lines: EC behavior under illumination. Dashed lines: EC behavior in the dark. As predicted from the interface investigations the samples show different behaviors depending on the surface barrier height.

native oxide the electrochemical performance can be assumed to be improved.

In addition, all the samples show a strongly improved behavior compared to the p-Si | Cu sample Figure 2. There are well defined photo current voltage curves and low dark current curves as expected for a diode in the reverse saturation potential regime. Furthermore, the photo current onset is shifted from about −0.7 V to 0.0 V vs. RHE in the best case which is in good agreement to the photo voltage expected for the pn^+-Si junction with the given doping concentration.

Conclusions

(100) pn^+-Si junctions with three different surface terminations (hydrogen, 3 Å native oxide and 7 Å thermal oxide) were covered with Cu as catalytically active layer for the CO_2 reduction reaction. The interfaces of all model systems were investigated by XPS and the electrochemical performances were measured by cyclic voltammetry in comparison to the bare p-Si | native SiO_2 junction. The interface experiments clearly show, that the optimum band alignment was achieved with the pn^+-Si | thermal SiO_2 | Cu sample with a band bending of only 0.27 eV in the n^+ layer followed by the pn^+-Si | native SiO_2 | Cu sample with a band bending of 0.35 eV and 0.45 eV for the pn^+-Si:H | Cu sample. Thus, the surface passivation was most effective with a relatively thick intermediate thermal oxide layer of 7 Å. The pn^+-Si | thermal SiO_2 | Cu sample with the most favorable electron transport due to its band alignment was proven to also show the best electrochemical performance. While the pn^+-Si | thermal SiO_2 | Cu sample reached a current density of −2 mA/cm^2 with an applied potential of only −0.4 V, the pn^+-Si | native SiO_2 | Cu sample needed a potential of −0.6 V and the pn^+-Si:H | Cu sample −0.7 V. The p-Si | SiO_2 | Cu junction did not show any reasonable performance for all surface treatments tested for this interface. This shows that the energy level alignment is indeed critical for and directly linked to the electrochemical performance. By interface engineering, as demonstrated here for different Si terminations, an electrochemical system for CO_2 reduction can be investigated and successfully optimized based on the electronic structure.

As next step we will check if further improvements in the procedure of Cu deposition onto the n^+ Si layer by modified surface engineering processes or soft Cu deposition procedures will be possible. In addition other CO_2 reduction catalysts will be tested. Finally, Cu and alternative catalytic active layers will be deposited onto p-i-n-Si multiabsorber structures.

Acknowledgments

Financial support through the a-leaf project (732840-A-LEAF) by the European Union and by the DFG in the framework of the Darmstadt Graduate School of Excellence for Energy Science and Engineering (GSC 1070) is gratefully acknowledged.

ORCID

Céline Steinert https://orcid.org/0000-0002-4246-8635
Sven Tengeler https://orcid.org/0000-0003-3405-4229

References

1. M. Mishra and D. M. Chun, *Applied Catalysis A*, **498**, 126 (2015).
2. Y. Hori, *Modern Aspects of Electrochemistry No. 42*, Springer, (2008).
3. D. Ren, J. Fong, and B. S. Yeo, *Nature Communications*, **9**, 925 (2018).
4. Z. Weng, Y. Wu, M. Wang, J. Jiang, K. Yang, S. Huo, X. Wang, Q. Ma, G. W. Brudvig, V. S. Batista, Y. Liang, Z. Feng, and H. Wang, *Nature communications*, **4**, 415 (2018).
5. M. Gattrell, N. Gupta, and A. Co, *Journal of the Electroanalytical Chemistry*, **594**, 1 (2006).
6. K. P. Kuhl, E. R. Cave, D. N. Abram, and T. F. Jaramillo, *Energy & Environmental Science*, **5**, 7050 (2012).
7. F. Urbain, P. Tiang, N. M. Carretero, T. Andreu, L. G. Gerling, C. Voz, J. Arbiol, and J. R. Morante, *Energy & Environmental Science*, **10**, 2256 (2017).
8. G. J. Bullock, D. F. Srankó, C. M. Towle, Y. Lum, M. Hettick, M. C. Scott, A. Javey, and J. Ager, *Energy & Environmental Science*, **10**, 2222 (2017).
9. Y. Sugano, A. Ono, R. Kitagawa, J. Tamura, M. Yamagiwa, Y. Kudo, E. Tsutsumi, and S. Mikoshiba, *RSC Advances*, **5**, 54246 (2015).
10. J. T. Song, H. Ryoo, M. Cho, J. Kim, J. G. Kim, S. Chung, and J. Oh, *Advanced Energy Materials*, **7**, 1601103 (2017).
11. T. Arai, S. Sato, and T. Morikawa, *Energy & Environmental Science*, **8**, 1998 (2015).
12. R. Kuriki, K. Sekizawa, O. Ishitani, and K. Maeda, *Angewandte Chemie International Edition*, **54**, 2406 (2015).
13. J. Albo, M. Alvarez-Guerra, P. Castano, and Á. Irabien, *Green Chemistry* (2013).
14. D. W. DeWulf, T. Jin, and A. J. Bard, *Journal of the Electrochemical Society*, **136**(6), 1686 (1989).
15. Y. Hori, A. Murata, and R. Takahashi, *Journal of the Chemical Society, Faraday Transactions 1*, **85**(8), 2309 (1989).
16. M. Ma, K. Djanashvili, and W. A. Smith, *Angewandte Chemie International Edition*, **128**, 6792. (2016).
17. M. Azuma, K. Hashimoto, M. Hiramoto, M. Watanabe, and T. Sakata, *Journal of the Electrochemical Society*, **137**(6), 1772 (1990).
18. H. D. Jesús-Cardona, C. del Moral, and C. R. Cabrera, *Journal of the Electroanalytical Chemistry*, **513**(1), 45 (2001).
19. S. Tengeler, M. Fingerle, W. Calvet, C. Steinert, B. Kaiser, T. Mayer, and W. Jaegermann, *Journal of the Electrochemical Society*, **165**(4), H3122 (2018).
20. W. Kern, *Journal of the Electrochemical Society*, **137**(6), 1887 (1990).
21. W. Jaegermann, B. Kaiser, J. Ziegler, and L. Klett, *Photoelectrochemical Solar Fuel Production*, Springer, 1 ed. (2016).
22. S. Giménez, J. Bisquert, S. Tengeler, B. Kaiser, D. Chaussende, and W. Jaegermann, *Applied Surface Science*, **400**, 6 (2016).
23. M. P Seah and S. J. Spencer, *Surface and Interface Analysis*, **33**, 640 (2002).
24. D. A. Shirley, *Physical Review*, **5.12**, 4709 (1972).
25. F. J. Grunthaner, P. J. Grunthaner, R. P. Vasquez, B. F. Lewis, and J. Maserjian, *Journal of Vacuum Science and Technology*, **16**, 1443 (1979).
26. L. He, W. Zhou, D. Cai, S. S. Mao, K. Sun, and S. Shen, *Cataysis. Science & Technology*, **7**, 2632 (2017).
27. V. Lehmann and H. Föll, *Journal of the Electrochemical Society*, **135**(11), 2831 (1988).
28. M. Malizia, B. Seger, I. Chorkendorff, and P. C. K. Vesborg, *Journal of Materials Chemistry A*, **2**, 6847 (2014).
29. F. J. Himpsel, G. Hollinger, and R. A. Pollak, *Physical Review B*, **28**, 7014 (1983).
30. C. C. Hobbs, L. R. C. Fonseca, A. Knizhnik, V. Dhandapani, S. B. Samavedam, W. J. Taylor, J. M. Grant, L. R. G. Dip, D. H. Triyoso, R. I. Hegde, D. C. Gilmer, R. Garcia, D. Roan, M. L. Lovejoy, R. S. Rai, E. A. Hebert, H. Tseng, S. G. H. Anderson, and B. E. White, *IEEE Transactions on Electron Devices, Vol.* **51**, 6 (2004).
31. O. F. Sankey, R. E. Allen, and J. D. Dow, *Solid State Communications*, **49**(1), 1 (1984).
32. R. T. Tung, *Physical Review Letters*, **84**, 6078 (2000).
33. Prof. E. H. Rhoderick, M. A., M. Sc., Ph. D., C. Eng., and F. Inst. P., F. I. E. E. *IEEPROC*, **129**, Pt. I, No. 1 (1982).
34. J. F. Moulder, W. F. Stickle, P. E. Sobol, and K. D. Bomben, *Handbok of X. ray Photoelectron Spectroscopy, s. l. : Physical Electronics, Inc.*, 1995.
35. Z. H. Lu, J. P. McCaffrey, B. Brar, G. D. Wilk, R. M. Wallace, L. C. Feldman, and S. P. Tay, *Applied Physics Letters*, **71**, 2764 (1997).

36. D. F. Mitchell, K. B. Clark, J. A. Bardwell, W. N. Lennard, G. R. Massoumi, and I. V. Mitchell, *Surface and Interface Analysis*,**21**, 44 (1994).
37. S. K. Chawla, N. Sankarraman, and J. H. Payer, *Journal of Electron Spectroscopy and Related Phenomena*, **61**, 1 (1992).
38. Y. A. Teterin, K. E. Ivanov, A. Y. Teterin, A. M. Lebedev, I. O. Utkin, and L. Vukchevich, *Journal of Electron Spectroscopy and Related Phenomena*, **101–103**, 401 (1999).
39. M. C. Biesinger, L. W. M. Lau, A. R. Gerson, and R. S. C. Smart, *Applied Surface Science*, **257**, 887 (2010).
40. R. Padiyath, J. Seth, S. V. Babu, and L. J. Matienzo, *Journal of Applied Physics*, **73**, 2326 (1993).
41. M. Dai, J. Kwon, M. D. Halls, R. G. Gordon, and Y. J. Chabal, *Langmuir*, **26**(6), 3911 (2010).
42. J. P. Espinós, J. Morales, A. Barranco, A. Caballero, J. P. Holgado, and A. R. González-Elipe, *The Journal of Physical Chemistry, B*, **106**, 6921 (2002).
43. G. Panzner, B. Egert, and H. P. Schmidt, *Surface Science*, **151**, 400 (1989).